Available online at www.sciencedirect.com
ScienceDirect
Journal of Power Sources 178 (2008) 197–206
JOURNAL OF POWER SOURCES
www.elsevier.com/locate/jpowsour

# Equivalent circuit elements for PSpice simulation of PEM stacks at pulse load

Wenhua H. Zhu [a], Robert U. Payne [a], R. Mark Nelms [b], Bruce J. Tatarchuk [a,*]

[a] *Center for Microfibrous Materials Manufacturing, Department of Chemical Engineering, Auburn University, AL 36849-5127, USA*
[b] *Department of Electrical Engineering, Auburn University, AL 36849-5201, USA*

Received 12 October 2007; received in revised form 4 December 2007; accepted 5 December 2007
Available online 15 December 2007

**Abstract**

The PEFC stack in a commercial power system was operated with room air and pure hydrogen. After the system reached a steady temperature, an ac impedance test was conducted on the fuel cell power system. The impedance data were real-time response generated by the ac sinusoidal excitation. Data for a single PEM stack and PEM stacks operating in parallel and series were collected with or without an embedded system controller board and electronic devices. The equivalent circuit model with three time constants and the non-linear least square fitting program (NLLS) were applied for fitting the stack impedance spectrum. The Levenberg–Marquardt algorithm utilized in the NLLS fitting process automatically adjusted the parameter values of the physical elements in the model to find the best fit result. From the preliminary results, data interpretation and the equivalent circuit model identified the physical elements, the related electrochemical processes, and the phenomenon inside the fuel cells or stacks. Losses from ohmic conduction, anode activation, cathode activation, and mass transfer were separated and analyzed. Further PSpice simulation curves using these equivalent circuit elements demonstrate good agreement with the pulse testing data measured from the PEFC power system.


*Keywords:* Proton exchange membrane fuel cells; Ac impedance; Equivalent circuit model; PSpice pulse simulation; PEFC stack

## 1. Introduction

Proton exchange membrane (PEM) fuel cells directly and continuously convert the chemical energy of a reaction between gaseous fuel and gaseous oxidant into electrical energy. Determination of the fuel cell degradation, recoverable poisoning, state of single MEA health, and stability of long-term stack operation are challenges for current fuel cell investigation [1]. Most ac impedance work was conducted on the air electrode and cathode catalyst layer [2–4]. Dynamic ac impedance measurements are attractive as an in situ technique for fuel cell diagnostics and simulation [5]. Holz and Vielstich measured ac impedance data for Teflon-bonded oxygen porous electrodes of an alkali fuel cell [6]. This work developed an equivalent circuit containing resistors (solution resistance, charge transfer, and $O_2$ adsorption), capacitors (double layer capacitance and $O_2$ adsorption capacitance on catalyst), and Warburg impedances ($O_2$ and ion diffusion to catalyst). Springer applied ac impedance to the polymer electrolyte fuel cell (PEFC or PEMFC) including equation implementation, model simplification and versification, least squares fitting, and interpretation of impedance features [7]. Diard et al. conducted impedance measurement (load $R = 1\ \Omega$) of a 10 W four-cell HPower stack using pure $H_2$ and $O_2$ and estimated that the resistance of the polymer membrane was *ca*. 40% of the internal resistance [8]. Wagner examined the impedance spectra of a PEM fuel cell and simulated the measured EIS with an equivalent circuit in order to split the cell impedance into electrode impedances and electrolyte resistance by varying the operating current through load changes [9]. However, the physical elements were not analyzed and no proper values were given for these elements. Instead, it emphasized the correlation between impedance of the fuel cell and *i*–*V* curve. Wilkinson and St-Pierre [10] obtained some useful parameters with ac impedance separating kinetic, ohmic, and mass transport effects for PEM fuel cells using different gas compositions such as $O_2$, air, and 79% He/21% $O_2$.

* Corresponding author. Tel.: +1 334 844 2023.
*E-mail address:* brucet@eng.auburn.edu (B.J. Tatarchuk).

0378-7753/$ – see front matter © 2007 Elsevier B.V. All rights reserved.
doi:10.1016/j.jpowsour.2007.12.014

Yuan et al. performed impedance measurement of a 500 W six-cell PEM stack using hydrogen and air [11]. Impedance arcs including air mass transport and anode activation loss demonstrated the effects of air shortage at 30 °C and 50 °C. There is no doubt that the study of the whole PEM stack system with solid electrolyte membranes is extremely difficult if using a traditional reference electrode. Kuhn et al. [12] first introduced a pseudo reference electrode into the fuel cell for separation of the anode and cathode to study the anodic kinetic parameters.

Electrochemical impedance spectroscopy (EIS) is a powerful tool used to formulate a hypothesis when EIS data is fit to an equivalent circuit model. The number of circuit elements and types of circuit models are determined by a perfect fit using the curve-fitting software and suitable interpretation of the circuit models and physical elements. The "Goodness of fit" is a Chi-squared parameter ($\chi^2$), normally included in the curve-fitting software [13]. Boukamp recommended that after a new circuit element is introduced into the circuit model, the value of $\chi^2$ should decrease by tenfold [14]. If the result of an additional circuit element does not improve the goodness of fit, one should keep the simpler model, search for an improved circuit model, or use another circuit element.

Several circuit elements are usually used in the fuel cell circuit modeling. The Gerischer element describes a preceding chemical reaction in the bulk reaction and also can be applied to model the porous electrode process [15]. The most common and simplest diffusion circuit element to use is called the Warburg diffusion element [16]. It can be used to model semi-infinite linear diffusion, i.e. unrestricted diffusion to a large planar electrode. When a thin film process (finite diffusion) is involved in the reaction process, the O and T elements are useful for real diffusion simulation [13]. The constrained diffusion circuit element (O) is present in situations such as the rotating disk electrode when the electroactive species must diffuse to the electrode surface through a thin diffusion layer, outside of which the solution is well mixed. The constrained diffusion circuit element (T) is characteristic of a type of film which contains a fixed amount of electroactive substance, such as in batteries, supercapacitors, or conducting polymer membrane. For PEM fuel cells, mass transport happens only by diffusion in a region near to the electrodes, the "Nernst diffusion layer". The concentration of species outside of this layer is homogenous for a period of time. The fuel gas or oxygen has to diffuse through the Nernst diffusion layer to reach the active reaction sites on the electrode. The O circuit element is applied to describe this Nernst diffusion impedance. Gamry named this diffusion impedance as the "Porous Bounded Warburg" circuit element [17,18]. The $C_{pe}$ (constant phase element) is a non-intuitive element which reflects the response of a real-world system when the center of the impedance arc is located below the $Z_{re}$-axis. Smooth mercury electrodes do not have depressed semi-circle. In EIS experiments, replacing the capacitor with $C_{pe}$ can yield better fitting results in comparison with the fitted results obtained by using a pure capacitor, represented by a parallel plate condenser [19]. One physical explanation for the $C_{pe}$ element is that it is caused by electrode roughness. This can be seen at carbon electrodes with a distribution of active sites (with varying activation energies) on the surface [13]. Electrochemical impedance spectroscopy is a powerful diagnostic tool and plays an important role in basic understanding of dynamic electrochemical processes. This paper uses ac impedance as an in situ diagnostic tool to perform non-destructive tests and analysis for a single PEM stack and for PEM stack pairs operated in parallel or series. Through applying reasonably simulated curve fits to obtain the equivalent circuit elements, these physical elements are then put into the PSpice circuit in order to compare the tested pulse data with PSpice simulation results.

## 2. Experimental

The purpose of this work originally started as a way to use various electrochemical methods to evaluate a real-world fuel cell system. Except for the current–voltage ($i$–$V$) curve, the diagnostics using the EIS impedance technique can obtain more useful parameters about the PEM fuel cell system at load. Impedance data need fit to an equivalent circuit diagram containing different physical elements such as charge transfer resistances ($R_f$), ohmic series resistances ($R_s$), double layer capacitances ($C_{dl}$), and Nernst impedance ($R_N$–$C_N$), where $R_f$ is related to the anode and cathode activation kinetics, $R_s$ is related to the electrolytes, $C_{dl}$ is related to the surface area of the electrocatalysts on the anodes and cathodes, and $R_N$–$C_N$ are related to the additional diffusion step or contributed by production of liquid water or reactive intermediates. In this preliminary PEM stack work, the above physical elements are included for simplification purpose. More elements related to mass transport, reaction mechanism, or pseudo capacitance may be added into the equivalent circuit model in the near future in order to have a better description of the stack operating behavior. The Nexa$^{TM}$ fuel cell modules including the PEM stacks (Ballard Power Systems Inc., British Columbia, Canada) were bought for the experimental tests. The fuel cell system is a small, low maintenance, fully automated, and highly integrated system. It provides 1200 W of unregulated dc power. Its output current can reach up to 44 A and stack voltage for 47 total fuel cells normally rises up to 41 V open-circuit. The fuel cell geometric working area is estimated as *ca.* 122 cm$^2$ due to the inexistence of manufacturing data. The automated operation is maintained by an embedded controller board. Some tests were performed by electrically isolating the PEM stack from the controller board to obtain pure stack impedance data. After starting the fuel cell system according to the manufacture's procedure, isolation was accomplished by connecting the board to an external power supply and the fuel cell stack was then ready for testing. At this point, an ac impedance experiment only probes the whole fuel cell stack except for the voltage tabs. For the preliminary test and impedance data measurement, this is a good approximation. Since voltage tabs are normally designed to have minimal electrical impact (high impedance) on the system under investigation, their effects are negligible to the impedance measurements. The PEM stack was then operated for collecting the

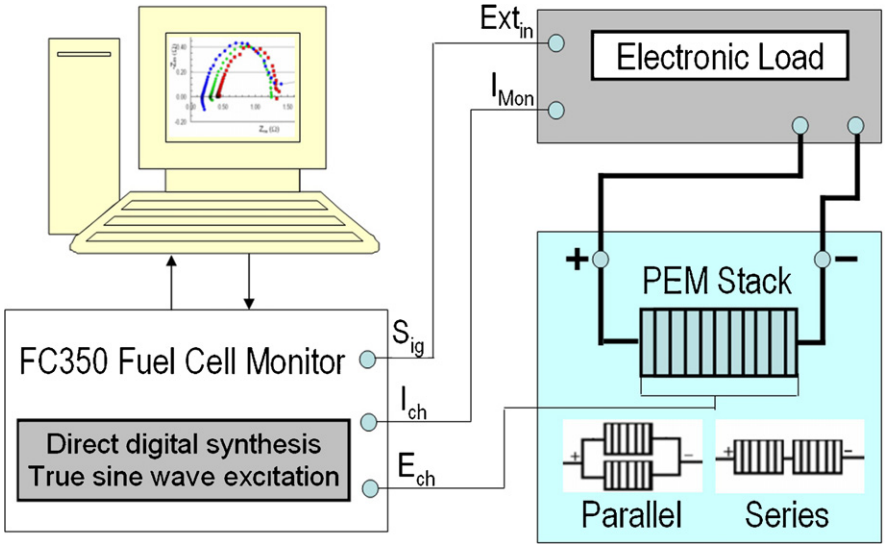


Fig. 1. Diagram of ac impedance data measurement from a Gamry FC350$^{TM}$ fuel cell monitor and an electronic load. Single fuel cell stack or PEM stacks in parallel/series arrangement.

ac impedance data at different current levels after being separated from the control subsystem. The supply pressures to the stack were 5.0 psig for hydrogen fuel and 2.2 psig for air oxidant. The fuel cell system was air cooled and had an attached humidity exchanger using exhaust water as a humidity resource [20].

The Gamry FC350$^{TM}$ fuel cell monitor (Gamry Instruments Inc., Warminster, PA) with a proper electronic load (Fig. 1) is available to work at a higher current range for measuring ac impedance data [21]. The contact and wire resistance between the power output wires and the testing fuel cell power source was approximately measured using *i–V* technique at different current levels. The true sine wave signal from the FC350$^{TM}$ system, working in galvanostatic or hybrid impedance mode, modulated the current from a single cell, multiple fuel cells, or the PEM stack(s). Simultaneously, the current information at the electronic load was sent to the computer, and the fuel cell voltage was also measured by the FC350$^{TM}$ monitor directly. The Gamry system collected these values and generated the impedance data for further analysis. In addition, a calibration process was applied to the Gamry FC350$^{TM}$ impedance system after it was set up. The system was connected with an external resistive dummy cell. The universal dummy cell is a 2 kΩ 0.05% accurate resistor in the position marked "calibration". The Gamry framework provides a calibration script and the calibration process followed by the manual instructions after the system installation was finished. The framework software allows measurements to be performed in a galvanostatic manner and a hybrid mode. Traditional measurements are performed using constant RMS amplitude for the ac signal. The problem with this technique is that the impedance of the cell varies significantly from high to low frequencies. For impedance to be accurate, the perturbation signal has to be sufficiently small to maintain a pseudo-linear *i–V* operation. Hybrid measurements compensate for the change in cell impedance as frequency is varied by changing the ac current amplitude to keep measured ac voltage at a set value. The previously measured impedance point is used in determining the new current amplitude as the scan proceeds from 10 kHz to 10 mHz. In this work, the hybrid EIS mode was applied for the experiments in order to observe the EIS behavior at various frequencies. For the entire stack in the system, it was tested with and without the embedded controller. For the measured impedance spectrum, the Echem Analyst software [17] including a complete equivalent circuit modeling package was applied to find the model parameters for best agreement between the model impedance spectra and the measured data. The Levenberg–Marquardt algorithm was utilized in the NLLS fitting process.

The general circuit elements (L, R, and C) are applied to the equivalent circuit models for non-linear simulation. Because the PEM stack is much more complicated than the situation of a single cell, the circuit is kept as simple as possible. This simplification enables us to have better initial understanding of the stack behavior under operating conditions, because various impedance parameters and losses including anode, cathode, and membrane electrolyte change with different operating conditions and power output levels. After the equivalent circuit elements were obtained, these data can be further put into the PSpice circuit for pulse simulation. For the preliminary tests on stack evaluation and diagnostics, the circuit elements in the PSpice simulation are fitted to data obtained with the controller board and electronic devices in order to keep the simulation process simplified. A software package including MicroSim Schematics and Waveform Analyzer (MicroSim Corporation, Version 8.0) was utilized as the PSpice simulation tool. The stack was loaded with different current amplitudes at a 20% duty cycle and 200 Hz frequency. Pulse test data for the stack(s) were collected using the PLZ electronic load and an AWG710 Tektronix digital oscilloscope.

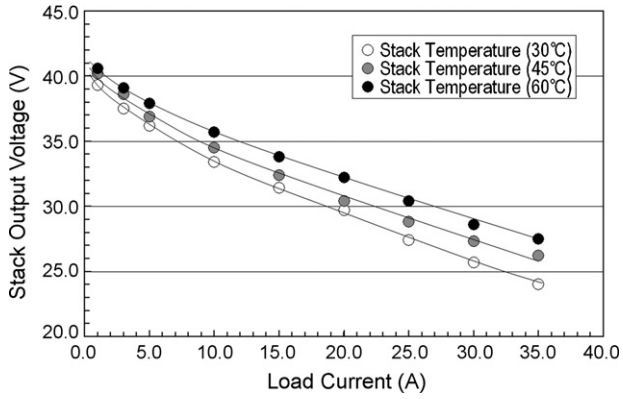


Fig. 2. Polarization curves measured from the BPS Nexa$^{TM}$ stack with periodic current interruption to maintain isothermal stack temperature.

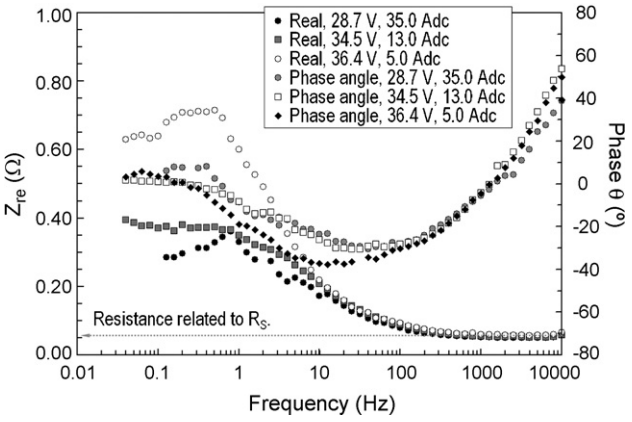


Fig. 3. Bode plots of the PEM stack #515 embedded with system controller, compressor, and other electronic devices in the Nexa$^{TM}$ power module. The voltage and current in the graph is the value just beginning of the impedance test startup, and the hybrid mode uses 150 mV ac.

## 3. Results and discussion

### *3.1. Stack current–voltage curves through periodic current interruption*

For a PEM stack in a fully automated and highly integrated system, it is extremely difficult to maintain an isothermal stack temperature in order to obtain the current–voltage curves for stack characterization. The periodic current interruption method was applied to the lab test for approximately evaluating the current–voltage curves [22]. The stack output voltage is a function of the operating current (Fig. 2). The stack output voltage is higher with increasing stack temperature. For a more accurate evaluation, an external power source may be used to provide the power for the stack's system controller board, compressor, and other electronic devices. The standard *i–V* curves can be obtained based on the fuel cell working area, which was estimated as *ca.* 122 cm$^2$ due to the inexistence of manufacturing data.

### *3.2. Stack impedance data and simulation*

The stack #515 was operated until it reached its steady state at a certain current level. Then, impedance data were collected by the Gamry system at various frequencies from 10 kHz to 10 mHz. The impedance test is normally stopped once data is out of the normal test range and not acceptable. The Bode plots are shown in Fig. 3, i.e. real part of impedance and phase angle shift are plotted as functions of frequency. The measured ohmic series resistance ($R_s = 55\,m\Omega$) related to the membrane electrolyte is clearly indicated in Fig. 3. The simulated average value for the ohmic series resistance, $\overline{R_s} = 52\,m\Omega$ ($\overline{R_s} = \sum_{i=1}^{n} R_{s,i}$, Table 1), is well matched with the measured data. As shown in Table 1, the measured ohmic series resistance ($\overline{R_s} = 70\,m\Omega$) is increased due to changing the power source for the embedded electronic devices from the fuel cell stack to the external power source. The wire and contact resistance ($R_W$) was determined by measuring the voltage drop at a specified current. The stack ohmic resistance including membrane electrolyte resistance is $R_{El} = R_s - R_W$. In connection with the ohmic series resistance value with embedded control devices, the total resistance for the controller board, compressor and other electronic devices can be estimated by Ohm's law. The ohmic resistance of the control circuit in parallel with the PEM stack can be determined in the high frequency region where the capacitance is viewed as a wire and the circuit is simplified. This resistance is a useful parameter for the PEM system evaluation.

The Nyquist plots are shown in Fig. 4a and b including both measured data and simulated curves. The circuit model of *LR*(*RC*)(*RC*)(*RC*) is applied to all impedance data simulation for the stack #515 and the stack #881. At the high frequency side of the half semi-circle as shown in Fig. 4a, the simulated curves are matched well with the measured data. But at low frequency side near the $Z_{re}$-axis, the simulated Nyquist curves are not identical with the measured data, especially at smaller currents of 5 A or 8 A when the PEM stack is connected to the control devices. This noise is caused by the control devices as evidence by comparing Fig. 4a with the result after the control devices disconnected from the PEM stack and powered by an external power source (Fig. 4b). After the control devices are isolated from the stack

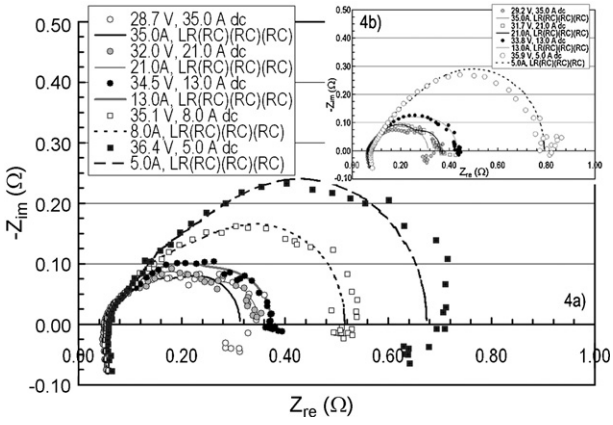


Fig. 4. Nyquist plots of the PEM stack #515 in the Nexa$^{TM}$ PEM system. The voltage and current in the graph is the value just beginning of the impedance test startup, and the hybrid mode uses 150 mV ac. (a) The PEM stack is equipped with embedded system controller, compressor, and other electronic devices; (b) the PEM stack is running while its controller board and other electronic devices uses an external power source. The simulated curves in all figures using *LR*(*RC*)(*RC*)(*RC*) circuit model.

Table 1
Simulated physical elements and values of the PEM stacks #515 and #881 using the $LR(RC)(RC)(RC)$ equivalent circuit

| Load current (A) | Physical interpretation | | | | | | | | | Levenberg–Marquardt method |
|---|---|---|---|---|---|---|---|---|---|---|
| | Wiring inductance | Ohmic series resistance | | Cathode activation kinetics and Nernst impedance related to the additional step | | | | Anode activation kinetics | | Goodness of fit |
| | $L_0$ [$L_0$] (μH) | $R_s$ [$R_s$] (mΩ) | $R_{El}$ (mΩ) | $R_{f,C}$ [$R_1$] (mΩ) | $C_{dl,C}$ [$C_1$] (mF) | $R_N$ [$R_2$] (mΩ) | $C_N$ [$C_2$] (mF) | $R_{f,A}$ [$R_3$] (mΩ) | $C_{dl,A}$ [$C_3$] (mF) | |
| With control board and electronic devices (FC #515) | | | | | | | | | | |
| 5 | 1.158 | 58.00 | 66.23 | 133.2 | 73.04 | 438.3 | 145.8 | 44.78 | 21.94 | 2.973E−03 |
| 8 | 1.155 | 54.45 | – | 133.8 | 66.58 | 283.5 | 186.8 | 43.84 | 20.45 | 1.671E−03 |
| 13 | 1.198 | 53.11 | 60.28 | 152.6 | 70.40 | 119.5 | 551.7 | 48.23 | 21.04 | 1.024E−03 |
| 21 | 1.144 | 49.80 | 57.37 | 144.2 | 75.25 | 107.3 | 1023 | 48.06 | 21.04 | 1.432E−03 |
| 26[a] | 1.150 | 48.11 | – | 130.3 | 70.37 | 109.5 | 806.6 | 43.23 | 20.76 | – |
| 28 | 1.152 | 47.44 | 54.78 | 124.8 | 68.43 | 110.4 | 720.0 | 41.30 | 20.65 | 2.449E−03 |
| 35 | 0.6956 | 50.35 | 53.16 | 105.1 | 63.69 | 127.9 | 389.8 | 29.86 | 29.53 | 4.966E−03 |
| Without control board and electronic devices (FC #515) | | | | | | | | | | |
| 5 | 0.9166 | 77.91 | 66.23 | 141.5 | 67.91 | 538.4 | 126.2 | 33.87 | 19.25 | 1.526E−03 |
| 13 | 0.8550 | 71.96 | 60.28 | 174.2 | 58.31 | 152.9 | 367.3 | 33.06 | 21.02 | 1.151E−03 |
| 21 | 0.8186 | 69.05 | 57.37 | 159.1 | 61.90 | 31.87 | 908.0 | 31.60 | 24.58 | 1.650E−03 |
| 28 | 0.8381 | 66.46 | 54.78 | 136.6 | 63.65 | 109.3 | 889.6 | 29.06 | 25.16 | 1.981E−03 |
| 35 | 0.8455 | 64.84 | 53.16 | 103.1 | 61.65 | 103.4 | 407.9 | 22.94 | 24.95 | 4.23E−03 |
| With control board and electronic devices (FC #881) | | | | | | | | | | |
| 5 | 0.7433 | 61.85 | – | 135.3 | 81.21 | 523.6 | 151.7 | 47.69 | 23.69 | 3.70E−03 |
| 6 | 0.7246 | 61.99 | 68.30 | 135.7 | 82.68 | 432.2 | 165.9 | 47.59 | 23.64 | 2.560E−3 |
| 8 | 0.7315 | 59.83 | 66.14 | 123.0 | 77.16 | 371.7 | 173.4 | 43.54 | 23.73 | 1.576E−3 |
| 13 | 0.7330 | 58.05 | 63.87 | 138.6 | 77.82 | 236.1 | 256.4 | 42.79 | 24.95 | 1.426E−3 |
| 21 | 0.7395 | 55.41 | 60.05 | 178.3 | 91.02 | 135.2 | 1234 | 52.56 | 26.42 | 1.901E−3 |
| 26[a] | 0.7340 | 54.20 | 58.60 | 141.5 | 90.11 | 160.6 | 757.4 | 46.65 | 27.63 | – |
| 28 | 0.7318 | 53.71 | 58.03 | 126.8 | 89.74 | 170.8 | 566.8 | 44.29 | 28.12 | 2.196E−3 |
| 35 | 0.7392 | 51.54 | 55.95 | 96.81 | 59.73 | 233.7 | 288.7 | 25.66 | 27.19 | 8.468E−3 |
| Without control board and electronic devices (FC #881) | | | | | | | | | | |
| 6 | 0.8805 | 79.98 | 68.30 | 113.5 | 66.51 | 487.8 | 140.6 | 30.89 | 17.68 | 1.956E−3 |
| 8 | 0.8900 | 77.82 | 66.14 | 111.8 | 68.07 | 392.3 | 153.1 | 30.04 | 18.73 | 1.799E−3 |
| 13 | 0.9007 | 75.55 | 63.87 | 117.7 | 68.61 | 257.0 | 204.8 | 29.41 | 21.15 | 1.230E−3 |
| 21 | 0.8724 | 71.73 | 60.05 | 162.9 | 82.43 | 157.1 | 847.9 | 37.25 | 26.48 | 1.380E−3 |
| 28 | 0.8735 | 69.71 | 58.03 | 169.2 | 99.90 | 211.3 | 1216 | 44.09 | 27.06 | 3.865E−3 |
| 35 | 0.8987 | 67.63 | 55.95 | 103.6 | 78.72 | 214.6 | 336.0 | 26.87 | 25.20 | 5.314E−3 |

Circuit simulation elements are represented in the square brackets.

[a] The values of the equivalent circuit elements at a specified load current were estimated based on the linear interpolation.

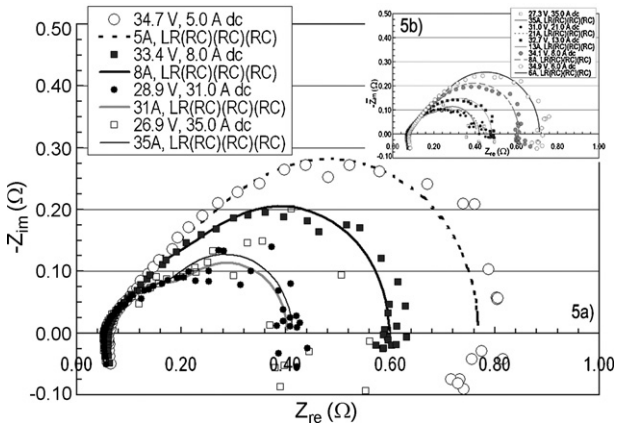


Fig. 5. Nyquist plots of the PEM stack #881 in the Nexa$^{TM}$ PEM system. The voltage and current in the graph is the value just beginning of the impedance test startup, and the hybrid mode uses 150 mV ac. (a) The PEM stack is equipped with embedded system controller, compressor, and other electronic devices; (b) the PEM stack is running while its controller board and other electronic devices uses an external power source. The simulated curves in all figures using *LR*(*RC*)(*RC*)(*RC*) circuit model.

power, the measured data are slightly depressed below the simulated curve at a load current of 5 A. Another stack #881 exhibits the similar behavior as shown in Fig. 5. Although measured data are basically matched with the simulated curves, the equivalent circuit model still needs improvement to sensitively describe the phenomena of air diffusion limitation on the cathode side. The values of simulated physical elements are shown in Table 1 according to the measured impedance data. The physical interpretation for the simulated elements is also listed for two stacks in this table. The stack ohmic resistance (bipolar plate contact and membrane electrolyte resistance) can be determined by the measured ohmic series resistance excluding the wiring and contacting resistance after the control devices were switched to an external power source. After the stack's ohmic, wire and contact resistances were determined, the control device's resistance could be calculated if necessary. The anode resistance relating to the activation kinetic loss was easily distinguished by considering a much lower anode resistance, identified as $R_{f,A}$ in Table 1. Because the catalyst loading level at the cathode side is reasonably 2–3 times higher than that at the anode side [23], it is not difficult to determine the cathode resistance (capacitance) related to its activation kinetic loss when the cathode side resistance (capacitance) is still assumed as 2–3 times higher than the anode side resistance (capacitance), identified as $R_{f,C}$ in Table 1. The other group of *RC* in the circuit corresponds to a finite diffusion step which is called a 'Nernst impedance' [9,24]. This is considered to be a frequency behavior related to a higher load of the fuel cell where there is a finite diffusion overvoltage. Wagner and co-workers use the third *RC* circuit near to the low frequency side to describe the high current density behavior. From this work as shown in Fig. 4b, it reveals that it is not well matched between the measured data and the simulated curves. The experimental data show that air-cathode diffusion losses gradually increase with operating current from 5 A to 13 A (*ca.* 41–107 mA cm$^{-2}$, Fig. 4). This may be generally considered as Wagner's finite diffusion over-voltage. However, the simulated Nyquist plots especially at the third *RC* circuit are well matched with the measured impedance data from 21 A to 35 A (*ca.* 172–287 mA cm$^{-2}$). The air-cathode diffusion loss in the testing PEM stack is considered to be almost half of the total losses when the stack is running within the above current densities. As a whole, the 3*RC* circuit related simulation curves approximately describe the behavior of different series ohmic resistance, activation and diffusion losses. But from 5 A to 13 A (30–39 °C), it is not clear why the diffusion losses at the air cathode are not fitting well with the simulated curves, which is called a "knot" feature. The rest of the third *RC* circuit curve near to the lower frequency side is considered as the finite diffusion loss (overvoltage). The model needs further consideration on describing that the air-cathode diffusion loss increases with operating current densities, because more air is necessary to diffuse into the cathode reactions while more nitrogen and water needs to be transferred to the exhaust channels.

At a current of 35 A (*ca.* 287 mA cm$^{-2}$), the measured impedance data are scattered and not well matched with simulated curves, mainly at the low frequency side. This is considered to be caused by liquid water production and removal from the cathode reaction zone. Water in liquid phase may plug the pores or diffusion channels and may also flood the active reaction sites at a high load current, because at a low load current the PEM stack uses much less hydrogen fuel and air oxidant producing less water and yielding a smooth-loop Nyquist plot. At the reaction zone, protons are recombining with adsorbed oxygen, and then water and heat are produced. Generated water removal further promotes mass transport at the reaction site. Water transport including phase change caused by heat transfer greatly promotes water and nitrogen transfer from the reaction zone to the exhaust channel. The adjustment of the active reaction sites (flooded or non-flooded, active or non-active) possibly changes the Nernst impedance which is mostly related to cathode side mass transport losses. As a whole, the knot features are observed in these Nyquist plots, especially for the last third of the loop at the low frequency side when operating at a lower current level (5–6 A individual stack, 10 A for stacks in parallel and 5 A for stacks in series). The preliminary explanation is that this feature is potentially caused by the air cathodes, possibly by the production of liquid water or the reactive intermediates. At low current levels, this phenomenon is obvious, and the simulation results deviate more at the low frequency side. At higher current level operation, the knot feature is not obvious, because of the increasing driving force for mass transfer and the balance between reactant diffusion and product removal. Although there are some unstable impedance data points, the simulation curves are well matched with the experimental data. The general equivalent circuit model is the main purpose for this work. Better understanding of these knot features may be obtained through the use of better instrument techniques and experimental improvements.

### 3.3. Stack operation in parallel

When two Nexa$^{TM}$ PEM stacks were operated in parallel, two power systems were assumed as one power source. The ac

Table 2
Simulated physical elements and values of the PEM stack #515 co-operated with the PEM stack #881 using the *LR*(*RC*)(*RC*)(*RC*) equivalent circuit

| Load current (A) | Physical interpretation | | | | | | | | Levenberg–Marquardt method |
|---|---|---|---|---|---|---|---|---|---|
| | Wiring inductance | Ohmic related series resistance | Cathode activation kinetics and Nernst impedance related to the additional step | | | | Anode activation kinetics | | Goodness of fit |
| | $L_0$ [$L_0$] (μH) | $R_s$ [$R_s$] (mΩ) | $R_{f,C}$ [$R_1$] (mΩ) | $C_{dl,C}$ [$C_1$] (mF) | $R_N$ [$R_2$] (mΩ) | $C_N$ [$C_2$] (mF) | $R_{f,A}$ [$R_3$] (mΩ) | $C_{dl,A}$ [$C_3$] (mF) | |
| Two stacks in parallel with control board and electronic devices (#515\|881) | | | | | | | | | |
| 10 | 1.157 | 38.82 | 63.83 | 156.1 | 229.8 | 287.5 | 26.28 | 34.63 | 1.942E−03 |
| 21 | 1.139 | 33.75 | 69.17 | 129.2 | 127.8 | 430.5 | 22.70 | 36.17 | 1.224E−3 |
| 26[a] | 1.141 | 32.78 | 70.27 | 133.3 | 100.5 | 806.3 | 24.04 | 36.63 | – |
| 30 | 1.142 | 32.00 | 87.36 | 136.5 | 78.74 | 1107 | 25.12 | 36.99 | 1.130E−3 |
| 40 | 1.138 | 31.44 | 79.24 | 156.2 | 72.06 | 1492 | 25.62 | 39.94 | 1.686E−3 |
| 50 | 1.158 | 31.56 | 71.73 | 153.0 | 84.33 | 1411 | 22.48 | 43.91 | 2.754E−3 |
| 60 | 1.182 | 30.79 | 61.20 | 148.4 | 89.87 | 1019 | 19.99 | 45.75 | 3.877E−3 |
| Two stacks in series with control board and electronic devices (#515–881) | | | | | | | | | |
| 5 | 4.120 | 155.5 | 264.3 | 41.63 | 834.1 | 78.62 | 107.4 | 9.314 | 3.690E−03 |
| 10 | 4.168 | 136.3 | 360.2 | 40.47 | 437.0 | 185.7 | 118.5 | 9.009 | 4.050E−03 |
| 13[a] | 4.217 | 132.0 | 362.2 | 40.41 | 360.3 | 284.5 | 116.1 | 9.354 | – |
| 15 | 4.250 | 129.1 | 363.6 | 40.37 | 309.1 | 350.3 | 114.5 | 9.584 | 4.840E−03 |
| 21 | 4.210 | 125.1 | 308.7 | 42.03 | 309.8 | 350.3 | 103.5 | 10.16 | 5.781E−3 |
| 25 | 4.222 | 121.7 | 231.2 | 37.47 | 338.3 | 214.4 | 89.24 | 9.843 | 5.689E−3 |
| 30 | 4.248 | 122.3 | 247.4 | 40.12 | 378.9 | 286.2 | 86.64 | 10.55 | 7.719E−3 |

Circuit simulation elements are represented in the square brackets.

[a] The values of the equivalent circuit elements at a specified load current were estimated based on the linear interpolation.

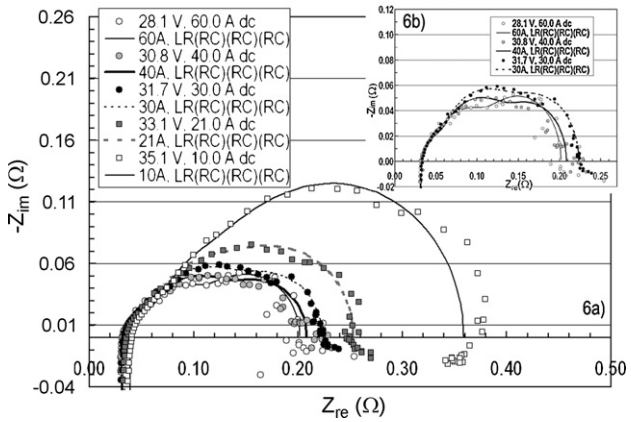


Fig. 6. Nyquist plots of the PEM stacks #515 and #881 in parallel operation embedded with system controller, compressor, and other electronic devices. The voltage and current in the graph is the value just beginning of the impedance test startup, and the hybrid mode uses 150 mV ac. (a) Operating current ranging from 10 A to 60 A; (b) enlarged Nyquist plots at higher current from 30 A to 60 A.

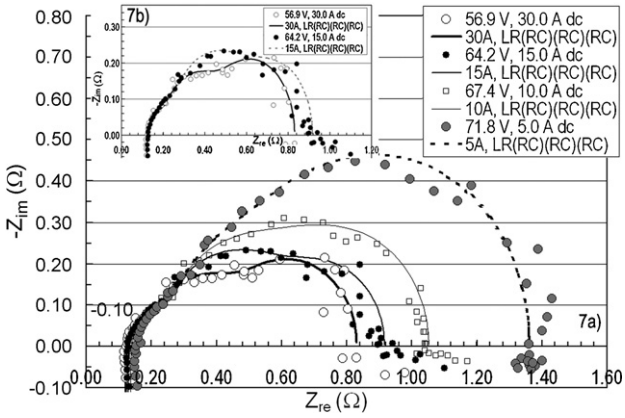


Fig. 7. Nyquist plots of the PEM stacks #515 and #881 in series operation embedded with system controller, compressor, and other electronic devices. The voltage and current in the graph is the value just beginning of the impedance test startup, and the hybrid mode uses 150 mV ac. (a) Operating current ranging from 5 A to 30 A; (b) enlarged Nyquist plots at higher current from 15 A to 30 A.

impedance measurement was conducted for the whole parallel stacks. The 3*RC* circuit model is still applied for simulation of two parallel stacks. The values of the simulated physical elements are shown in Table 2. The Nernst impedance is much higher than the cathode and anode impedance according to the analysis for the single PEM stack. Starting from a 30 A load, the cathode activation kinetic loss slightly decreases and the Nernst impedance loss gradually increases, which is identical behavior to the single stack's Nernst impedance at higher current operation. The Nyquist plots of the PEM stacks in parallel operation are shown in Fig. 6. The simulated Nyquist curves have similar results to the single tested PEM stack. The air-cathode mass transport loss starts to increase from 10 A to 21 A current at operational load. The impedance data describing cathode mass transport (the second part of the impedance loop) gradually matches with the Nyquist plots using the *LR*(*RC*)(*RC*)(*RC*) circuit model after it is loaded with 21 A current or higher. After a load of total 30 A (*ca.* 15 A for each stack, current each stack is different due to different stack impedances), the simulated Nyquist curves are identical with the measured impedance data (Fig. 6b). The 3*RC* circuit model still needs further improvement at low current levels, especially for the process simulation when the cathode Nernst impedance starts to increase in the parallel circuit.

### 3.4. Stack operation in series

Two Nexa$^{TM}$ power systems were operated in series. Two PEM stacks embedded with control board and electronic devices were assumed as one power source and ac impedance measurement was conducted for two series stacks. A voltage divider was applied for ac measurement due to the 50 V limitation of the Gamry system. The 3*RC* circuit model is applied for simulation of two series stacks, similar to the parallel operation. The values of the simulated physical elements are shown in Table 2. The Nernst impedance is much higher than the cathode and anode impedance. Starting from a 15 A load for each stack, the cathode activation kinetic loss slightly decreases and the Nernst impedance loss gradually increases, which is identical behavior to the single stack's Nernst impedance at higher current operation. The Nyquist plots of the PEM stacks in series operation are shown in Fig. 7b. The simulated Nyquist curves have the similar results as the single tested PEM stack. The increased cathode mass transport loss gradually matches with the *LR*(*RC*)(*RC*)(*RC*) circuit model curves since it starts a load of 15 A current. At a load of 30 A for stack pairs in series, the simulated Nyquist curves mainly reflect the effect of the cathode Nernst impedance (Fig. 7). The anode exhaust build-up and associated periodic purge may also cause the data points' fluctuations around the simulated curves. This anode mass transport limitation has been demonstrated when ac impedance tests included the purge cells where the anode exhaust builds up and less hydrogen fuel exists [25]. The cathode mass transport loss (or called Nernst impedance) is not visible when operating at low current levels in the series circuit.

### 3.5. PSpice simulation versus experimental data

SPICE is a powerful general purpose analog circuit simulator that is used to verify circuit designs and to predict the circuit behavior. This is of particular importance for integrated circuits as its name implies: Simulation Program for Integrated Circuits Emphasis [26]. PSpice is a SPICE analog circuit simulation software that runs on personal computers. It was developed by MicroSim and used in electronic design automation or simulation, providing industry-standard solutions for accurate analog and mixed-signal simulations such as non-linear transient analysis which calculates the voltage and current as a function of time when a large signal is applied. PSpice is a full-featured, mixed-signal simulator [27]. It is a useful tool to improve design performance, yield, and reliability. All analyses can be done at different temperatures.

A TDI electronic load was applied for the initial pulse test. Pulse ringing was observed at higher current pulse load. Three lead acid batteries (total voltage, 37.2 V) and a resistive elec-

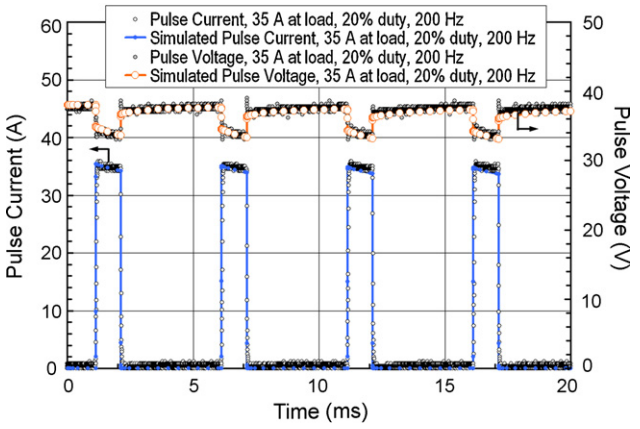


Fig. 8. Pulse current and voltage in comparison of PSpice simulation results for the stack #515 at load. Current 35 A, duty 20%, and test frequency 200 Hz.

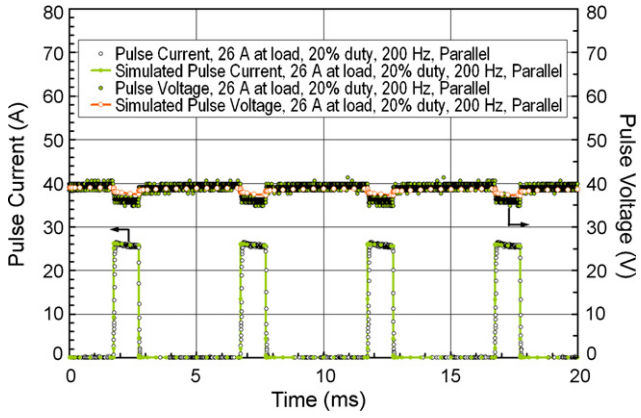


Fig. 9. Pulse current and voltage in comparison of PSpice simulation results for the stacks #515 and #881 in parallel operation at load. Current 26 A, duty 20%, and test frequency 200 Hz.

tronic load (PLZ-1003W, 1 kW, Kikusui Electrics Corporation) were chosen for further pulse test in order to determine from where the pulse noise came. Test results show that the TDI electronic load is an inductive load and is not proper for the pulse tests. The pulse tests for the stack(s) were conducted through the constant current mode and data were collected using a digital oscilloscope. The tested pulse voltage and current for the single stack #515 are compared with the PSpice simulation results, as shown in Fig. 8. The simulated curves are well matched with the pulse test data. The stacks #515 and #881 were then operated in parallel and series, separately. The measured pulse data and PSpice simulation results are independently shown in Figs. 9 and 10. For the impedance measurement and equivalent circuit model development, two stacks (#515 and #881) are assumed to be one bigger stack with featured stack parameters. For the parallel operation, the total impedance was smaller than either of two stacks. The simulated pulse curve has less voltage drop in comparison with the experimental pulse results. This error is possibly caused by measurement of the wire and contact resistance due to the smaller total parallel impedance. The location of the voltage probe is also important to the value of the pulse voltage. The series operation results are shown in Fig. 10. Due to higher voltage of two stacks, the peaks of the current pulse tend to be slightly slanted during measurement. In general, the PSpice

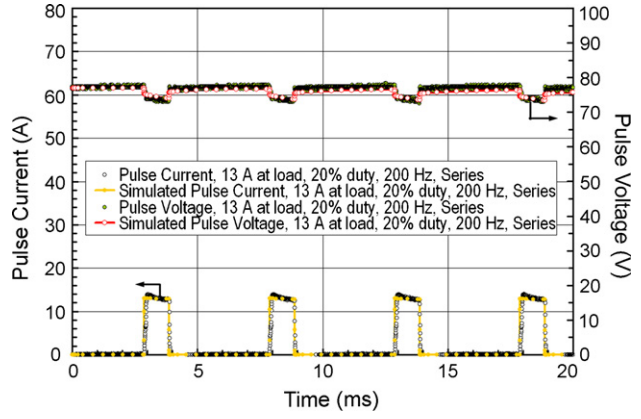


Fig. 10. Pulse current and voltage in comparison of PSpice simulation results for the stack #515 and #881 in series test at load. Current 13 A, duty 20%, and test frequency 200 Hz.

simulated pulse curves are well matched with the test pulse data.

The simulated electrochemical cell or stack behaviors through suitable physical elements in the equivalent circuit are potentially matched with the real-world reactions. No matter what type of reasonable circuit model in use, the PSpice simulation theoretically generates the same or similar results in the circuit diagram if essential physical circuit elements are properly

Table 3
Simulated pulse voltage at its peak current vs. the measured data value

| Two stacks #515 and #881 operating in parallel and series | Pulse voltage in parallel (V) | | | Pulse voltage in series (V) | | |
|---|---|---|---|---|---|---|
| | Start voltage at 0.01 A | Pulse voltage at a load of 26 A current[a] | Error (%) | Start voltage at 0.01 A | Pulse voltage at a load of 13 A current[a] | Error (%) |
| Simulated results of a two-individual stack circuit model | 39.00 | 37.83 | 4.50 | 77.00 | 74.60 | 1.17 |
| Simulated results of two stacks as one 3*RC* circuit model | 39.00 | 37.56 | 3.75 | 77.00 | 74.22 | 0.65 |
| Measured data values through digital oscilloscope | 39.08 | 36.20 | – | 77.06 | 73.74 | – |

[a] All simulated values and measured data were recorded at the second pulse voltage location. The average pulse voltage was calculated using the beginning, middle, and end values of the pulse voltage.

included and arranged in the circuit model. For better understanding of the individual stack model and the 3*RC* multi-stack circuit model, the relationship between single and multi-stacks is necessary for validation of the measurement method. In comparison with one simple 3*RC* circuit model for two stack pairs, the individual stack circuit model was also tested for the validation purpose. As listed in Table 3, both simulated results and measured data are generally well matched and the errors are between 0.65% and 4.5%. The relative errors for the parallel stack pairs are higher than that of stack pairs in series, because the power system in parallel has much lower impedance. The individual stack model deviates slightly more from experimental data in comparison to one 3*RC* circuit model. This is mainly caused by a lower error in the stack pairs, and the two-individual stack circuit is necessary to pay more attention on wire and contact resistances. The simulation deviation may be reduced further by better circuit model development and more accurate experimental measurements.

## 4. Conclusions

The PEFC stack in a commercial power system was successfully characterized by impedance measurements. Impedance data for single stack, parallel, and series stacks were obtained in the Nexa$^{TM}$ system with or without embedded system controller and other electronic devices. The equivalent circuit model with three time constants was developed using these real-time response data generated by ac sinusoidal excitation. Physical elements, electrochemical processes, and phenomenon inside the fuel cells or stacks were identified by further data interpretation. Losses from ohmic conduction, anode activation, cathode activation, and mass transfer were approximately separated and determined. Simulated pulse results from equivalent circuit elements and a PSpice tool demonstrate good agreement with the pulse data measured from the PEFC stack(s). Electrochemical impedance spectroscopy can serve as a diagnostic tool and perform non-destructive tests and analysis of the PEFC stacks and cells, especially for PSpice pulse simulation.

## Acknowledgements

The authors wish to acknowledge the contribution from Dr. Donald R. Cahela. Mr. Amar Tiwari is also appreciated for reading this manuscript.

## References

[1] N. Wagner, in: E. Barsoukov, J.R. Macdonald (Eds.), Impedance Spectroscopy-Theory, Experiment, and Applications, John Wiley & Sons, 2005, p. 498.
[2] S. Ahn, B.J. Tatarchuk, J. Electrochem. Soc. 142 (1995) 4169.
[3] M. Eikerling, A.A. Kornyshev, J. Electroanal. Chem. 107 (1999) 475.
[4] R. Makharia, M.F. Mathias, D.R. Baker, J. Electrochem. Soc. 152 (2005) A970.
[5] J.R. Selman, Y.P. Lin, Electrochim. Acta 38 (1993) 2063.
[6] R. Holz, W. Vielstich, J. Electrochem. Soc. 131 (1984) 2298.
[7] T.E. Springer, Electrochemical Society Proceedings, vol. 99-14, 1999, p. 208.
[8] J.P. Diard, N. Glandut, B.L. Gorrec, C. Montella, J. Electrochem. Soc. 151 (2004) A2193.
[9] N. Wagner, J. Appl. Electrochem. 32 (2002) 859.
[10] D.P. Wilkinson, N. St-Pierre, in: W. Vielstich, H. Gasteiger, A. Lamm (Eds.), Handbook of Fuel Cells—Fundamentals Technology and Applications, John Wiley and Sons, 2003, pp. 611–626.
[11] X. Yuan, J.C. Sun, M. Blanco, H. Wang, J. Zhang, D.P. Wilkinson, J. Power Sources 161 (2006) 920.
[12] H. Kuhn, B. Andreaus, A. Wokaun, G.G. Scherer, Electrochim. Acta 51 (2006) 1622.
[13] R.S. Rodgers, Research Solutions & Resources, 2005, http://www.consultrsr.com/resources/eis/index.htm.
[14] B.A. Boukamp, Solid State Ionics 18/19 (1986) 136.
[15] M. González-Cuenca, W. Zipprich, B.A. Boukamp, G. Pudmich, F. Tietz, Fuel Cells 1 (2001) 256.
[16] A.J. Bard, L.R. Faulkner, Electrochemical Methods—Fundamentals and Applications, John Wiley & Sons Ltd., Singapore, 1998, p. 376.
[17] Gamry Instruments, Gamry Echem Analyst Software—"Porous Bounded Warburg", 2007.
[18] Gamry Instruments, Electrochemical Impedance Spectroscopy Primer, Warminster, PA, 2007, p. 6.
[19] V.D. Jovic, Determination of the correct value of $C_{dl}$ from the impedance results fitted by the commercially available software, http://www.gamry.com, Warminster, PA, 2003.
[20] Ballard Power Systems, Nexa Power Module Installation Manual. British Columbia, Canada, 2002, pp. 1–49.
[21] Gamry Instruments, FC350$^{TM}$ Fuel Cell Monitor. Warminster, PA, 2002, pp. 1–4.
[22] W.H. Zhu, R.U. Payne, D.R. Cahela, B.J. Tatarchuk, J. Power Sources 128 (2004) 231.
[23] P. Costamagna, S. Srinivasan, J. Power Sources 102 (2001) 242.
[24] N. Wagner, E. Gulzow, B. Muller, M. Lang, Electrochim. Acta 43 (1998) 3785.
[25] W.H. Zhu, R.U. Payne, B.J. Tatarchuk, J. Power Sources 168 (2007) 211.
[26] Wikipedia Encyclopedia, Wikimedia Foundation Inc., 2007, http://en.wikipedia.org/wiki/PSPICE, http://en.wikipedia.org/wiki/SPICE.
[27] PSpice Simulation, Cadence Design Systems, San Jose, CA, 2007, http://www.cadence.com/products/orcad/pspice_a_d/index.aspx.